Compound waves in a thermohydrodynamic lattice BGK scheme using non-perturbative equilibria

P. J. Dellar(*)

Department of Applied Mathematics and Theoretical Physics, University of Cambridge, Silver Street, Cambridge CB3 9EW, UK

PACS. 47.40-x – Compressible flows; shock and detonation phenomena.
PACS. 05.20Dd – Kinetic theory.
PACS. 47.11+j – Computational methods in fluid dynamics.

Abstract. – A previously proposed thermohydrodynamic lattice BGK scheme using non-perturbative, or non-polynomial, equilibria is found to simulate continuum equations that differ from the Euler equations of gas dynamics at leading order. Shock tube simulations with this BGK scheme coincide with solutions obtained by solving these different continuum equations with conventional methods. Both sets of solutions contain unphysical compound waves, shocks attached to rarefactions, where the Euler equations contain contact discontinuities.

Lattice Boltzmann or lattice BGK equations [1–4] have proved successful at simulating nearly incompressible and isothermal fluid flows, for which they are a viable alternative to conventional numerical methods [5]. However, applications to flows with substantial temperature fluctuations have proved problematic. Many schemes are subject to instabilities, often attributed to the use of polynomial approximations for the equilibrium distributions. These equilibria may become negative, which violates the assumptions of a discrete H-theorem and may permit instability [5–8]. This has spurred recent work on constructing non-polynomial equilibria that remain positive, and often arise from extremising some entropy function [8–10].

Thermohydrodynamic flows are described most simply by the compressible Euler equations expressing conservation of mass, momentum, and energy – the last comprising both macroscopic kinetic energy, and internal kinetic energy or heat. The Euler equations are valid in the limit of high Reynolds number, when heat and momentum transport associated with molecular processes may be neglected. A more refined description requires the Navier-Stokes-Fourier equations that incorporate viscous and thermal diffusion.

In this Letter we investigate the thermohydrodynamic lattice BGK scheme proposed by Renda *et al.* [8], which uses "non-perturbative equilibria" in an attempt to maintain stability at higher Mach numbers. We show that this scheme simulates continuum equations that differ from the intended compressible Euler equations at leading order, due to an incorrect energy flux. Solutions of shock tube problems with this scheme contain unphysical compound

(*) Now at: OCIAM, Mathematical Institute, 24–29 St Giles', Oxford, OX1 3LB, UK.
Email: pdellar@na-net.ornl.gov

waves, shocks attached to rarefaction waves, where the Euler equations contain contact discontinuities. Compound waves cannot exist in the Euler equations, but may arise in more complicated physical systems such as magnetohydrodynamics [11].

Euler equations. – The Euler equations of gas dynamics may be written as a hyperbolic system expressing conservation of density ρ, momentum $\rho\mathbf{u}$, and energy E [12–14]

$$\frac{\partial}{\partial t}\begin{pmatrix}\rho\\ \rho\mathbf{u}\\ E\end{pmatrix}+\nabla\cdot\begin{pmatrix}\rho\mathbf{u}\\ \rho\mathbf{u}\mathbf{u}+p\,\mathsf{I}\\ \mathbf{u}(E+p)\end{pmatrix}=0, \tag{1}$$

where $\rho\mathbf{u}\mathbf{u}+p\,\mathsf{I}$ denotes the symmetric tensor with components $\rho u_\alpha u_\beta+p\delta_{\alpha\beta}$. The system is closed by the relation $E=p/(\gamma-1)+\frac{1}{2}\rho\,|\mathbf{u}|^2$, where γ is the ratio of specific heats. For a monatomic gas, $\gamma=1+2/D$ if the atoms are permitted to move in D spatial dimensions. Thus $\gamma=\frac{5}{3}$ for a real monatomic gas. For diatomic molecules $\gamma=\frac{7}{5}$, as used in aerodynamics, since the molecules' internal degrees of freedom act like two extra dimensions. It is often convenient to introduce a temperature θ so that $p=\theta\rho$. The energy is then $E=\frac{1}{2}\rho\,|\mathbf{u}|^2+\frac{1}{2}D\rho\,\theta$, naturally intepreted as the sum of macroscopic kinetic energy, and internal energy or heat.

Kinetic theory. – We recall that the Euler equations (1) may be derived by taking moments of the continuum Boltzmann-BGK equation [13–15]

$$\frac{\partial f}{\partial t}+\boldsymbol{\xi}\cdot\nabla f=-\frac{1}{\tau}\left(f-f^{(0)}\right). \tag{2}$$

Here $f(\mathbf{x},\boldsymbol{\xi},t)$ is the particle distribution function, proportional to the probability of finding a particle with microscopic speed $\boldsymbol{\xi}$ at position $\mathbf{x}$ at time t. The Bhatnagar-Gross-Krook (BGK) approximation [16] on the right hand side relaxes f towards the Maxwell-Boltzmann equilibrium distribution $f^{(0)}$ with timescale τ. This equilibrium is

$$f^{(0)}=\frac{\rho}{(2\pi\theta)^{D/2}}\exp\left(-\frac{(\boldsymbol{\xi}-\mathbf{u})^2}{2\theta}\right), \tag{3}$$

where ρ, $\mathbf{u}$ and θ are determined as moments of f (and of $f^{(0)}$ by construction) via

$$\rho=\int f\mathrm{d}\boldsymbol{\xi},\quad \rho\mathbf{u}=\int\boldsymbol{\xi}f\mathrm{d}\boldsymbol{\xi},\quad \rho\theta=\frac{1}{D}\int|\boldsymbol{\xi}-\mathbf{u}|^2f\mathrm{d}\boldsymbol{\xi}. \tag{4}$$

We work in units in which the particle masses and Boltzmann's constant are both unity, and velocities are scaled so that the isothermal sound speed $c_\mathrm{s}=\theta^{1/2}$. By taking $\int\mathrm{d}\boldsymbol{\xi}$, $\int\boldsymbol{\xi}\mathrm{d}\boldsymbol{\xi}$, and $\frac{1}{2}\int|\boldsymbol{\xi}|^2\mathrm{d}\boldsymbol{\xi}$ of equation (2) we obtain conservation equations in the form

$$\frac{\partial}{\partial t}\begin{pmatrix}\rho\\ \rho\mathbf{u}\\ E\end{pmatrix}+\nabla\cdot\begin{pmatrix}\rho\mathbf{u}\\ \boldsymbol{\Pi}\\ \mathbf{Q}\end{pmatrix}=0. \tag{5}$$

The right hand side vanishes because eqs. (4) hold for both f and $f^{(0)}$, thus expressing local mass, momentum, and energy conservation under collisions. The momentum flux $\boldsymbol{\Pi}$ and energy flux $\mathbf{Q}$ are given by

$$\boldsymbol{\Pi}=\int\boldsymbol{\xi}\boldsymbol{\xi}f\mathrm{d}\boldsymbol{\xi},\quad \mathbf{Q}=\frac{1}{2}\int\boldsymbol{\xi}\,|\boldsymbol{\xi}|^2f\mathrm{d}\boldsymbol{\xi}. \tag{6}$$

Equations (5) and (6) are an exact reduction from eq. (2), but the system is not closed until $\boldsymbol{\Pi}$ and $\mathbf{Q}$ are expressed in terms of the other variables. In the Chapman-Enskog expansion [15], based on small τ, or small mean free path, these fluxes are given at leading order by substituting $f = f^{(0)}$ into eq. (6). Equations (5) and (6) then reduce to the Euler equations (1). The $O(\tau)$ corrections from $f - f^{(0)}$ give a Navier-Stokes viscous stress, with viscosity $\mu = \rho\tau\theta$, and a Fourier diffusive heat flux at next order in the Chapman-Enskog expansion.

Lattice BGK. – Lattice BGK schemes are based on the fully discrete system

$$f_i(\mathbf{x} + \boldsymbol{\xi}_i\Delta t, t + \Delta t) - f_i(\mathbf{x}, t) = -\frac{1}{\tau}\left(f_i(\mathbf{x}, t) - f_i^{(0)}(\mathbf{x}, t)\right), \tag{7}$$

which resembles a finite difference approximation to eq. (2). The particle speed $\boldsymbol{\xi}$ is restricted to lie in a discrete set $\{\boldsymbol{\xi}_0, \boldsymbol{\xi}_1, \ldots, \boldsymbol{\xi}_N\}$, and we set $f_i(\mathbf{x}, t) = f(\mathbf{x}, \boldsymbol{\xi}_i, t)$. The density ρ, velocity $\mathbf{u}$, and temperature θ are given by discrete moments

$$\rho = \sum_{i=0}^{N} f_i, \quad \rho\mathbf{u} = \sum_{i=0}^{N} \boldsymbol{\xi}_i f_i, \quad \rho\theta = \frac{1}{D}\sum_{i=0}^{N} |\boldsymbol{\xi}_i - \mathbf{u}|^2 f_i, \tag{8}$$

instead of the integrals in eqs. (4). Similarly, the momentum and energy fluxes are given by

$$\boldsymbol{\Pi} = \sum_{i=0}^{N} \boldsymbol{\xi}_i\boldsymbol{\xi}_i f_i, \quad \boldsymbol{\Pi}^{(0)} = \sum_{i=0}^{N} \boldsymbol{\xi}_i\boldsymbol{\xi}_i f_i^{(0)}, \quad \mathbf{Q} = \sum_{i=0}^{N} \boldsymbol{\xi}_i |\boldsymbol{\xi}_i|^2 f_i, \quad \mathbf{Q}^{(0)} = \sum_{i=0}^{N} \boldsymbol{\xi}_i |\boldsymbol{\xi}_i|^2 f_i^{(0)}. \tag{9}$$

The lattice $\{\boldsymbol{\xi}_0, \boldsymbol{\xi}_1, \ldots, \boldsymbol{\xi}_N\}$ and the discrete equilibria $f_i^{(0)}$ must be chosen so that solutions of eq. (7) also approximate the desired hydrodynamics in the slowly varying ($\tau \to 0$) limit. In particular, $\boldsymbol{\Pi}^{(0)}$ and $\mathbf{Q}^{(0)}$ must be the momentum and energy fluxes from the Euler equations.

Non-perturbative equilibria. – The common three speed lattice BGK scheme [4, 5] simulates an isothermal fluid, with the energy equation replaced by a constant θ constraint. This is sufficient to simulate low Mach number flows, $\mathrm{Ma} = |\mathbf{u}|/c_\mathrm{s} \ll 1$, albeit with a non-zero bulk viscosity arising from a lack of local energy conservation [17]. At least five speeds are needed to simulate one dimensional gas dynamics with varying temperature. The most common choice uses $\xi_i = i \in \{-2, -1, 0, 1, 2\}$, in lattice units with $\Delta x = \Delta t = 1$. The three constraints

$$\sum_{i=-2}^{2} f_i^{(0)} = \rho, \quad \sum_{i=-2}^{2} \xi_i f_i^{(0)} = \rho u, \quad \sum_{i=-2}^{2} |\xi_i - u|^2 f_i^{(0)} = \theta\rho, \tag{10}$$

are insufficient to determine the $f_i^{(0)}$ uniquely (unlike the three speed case). Various choices based on polynomial expansions and fitting higher moments have been proposed [18], but they become unstable at quite modest Mach numbers. This instability is often attributed to the $f_i^{(0)}$ becoming negative when the fluid velocity is not sufficiently small [6–8]. Renda *et al.* [8] proposed a set of "non-perturbative" equilibria, intended to offer greater stability by remaining positive at moderate Mach numbers. They expressed the equilibria for the two fastest speeds, $f_{\pm2}^{(0)}$, as multiples of the two speed one equilibria $f_{\pm1}^{(0)}$,

$$f_2^{(0)} = \lambda_+ f_1^{(0)}, \quad f_{-2}^{(0)} = \lambda_- f_{-1}^{(0)}, \tag{11}$$

with multipliers $\lambda_\pm$ computed from the continuum Maxwell-Boltzmann distribution eq. (3),

$$\lambda_\pm = \exp\left[-\frac{(\pm2 - u)^2 - (\pm1 - u)^2}{2\theta}\right]. \tag{12}$$

The three constraints (10) are then sufficient to determine the equilibria uniquely,

$$f_{\pm1}^{(0)} = \rho\frac{(1+2\lambda_\mp)(u^2+\theta) \pm (1+4\lambda_\mp)u}{(1+2\lambda_+)(1+4\lambda_-)+(1+2\lambda_-)(1+4\lambda_+)}, \qquad f_0^{(0)} = \rho - (1+\lambda_+)f_1^{(0)} - (1+\lambda_-)f_{-1}^{(0)}. \tag{13}$$

The leading order one-dimensional momentum flux $\Pi^{(0)}$ is given correctly as

$$\Pi^{(0)} = \sum_{i=-2}^{2} \xi_i^2 f_i^{(0)} = \rho u^2 + \rho\theta, \tag{14}$$

due to the third of eqs. (10) and the vector identity $|\boldsymbol{\xi} - \mathbf{u}|^2 = |\boldsymbol{\xi}|^2 + |\mathbf{u}|^2 - 2\,\boldsymbol{\xi}\cdot\mathbf{u}$.

However, the leading order energy flux is incorrect, being the complicated expression

$$Q^{(0)} = \frac{1}{2}\sum_{i=-2}^{2} \xi_i^3 f_i = \frac{1}{2}(1+8\lambda_+)f_1^{(0)} - \frac{1}{2}(1+8\lambda_-)f_{-1}^{(0)} = \rho\Phi(u,\theta), \tag{15}$$

with $f_{\pm1}^{(0)}$ given by eq. (13), instead of $Q^{(0)} = u(p+E)$ as in eq. (1). The lattice BGK scheme with these equilibria therefore simulates the one-dimensional hyperbolic system

$$\frac{\partial}{\partial t}\begin{pmatrix} \rho \\ \rho u \\ \frac{1}{2}\rho u^2 + \frac{1}{2}\rho\theta \end{pmatrix} + \frac{\partial}{\partial x}\begin{pmatrix} \rho u \\ \rho u^2 + \theta\rho \\ \rho\Phi(u,\theta) \end{pmatrix} = 0, \tag{16}$$

at leading order, instead of the one-dimensional ($\gamma = 3$) Euler equations. The lattice BGK scheme with equilibria given by eqs. (13) and (11) was named the Maxwellian-closure BGK or MBGK scheme in [8], so we shall refer to the system (16), with Φ defined by eq. (15), that it simulates as the Maxwellian-closure partial differential equation or MPDE system.

Compound waves. – The MPDE system differs qualitatively from the Euler equations. The Jacobian matrix of the fluxes, as functions of the conserved variables $(\rho, \rho u, E)$, is

$$\begin{pmatrix} 0 & 1 & 0 \\ 0 & 0 & 2 \\ \Phi - u\Phi_u + (u^2-\theta)\Phi_\theta & \Phi_u - 2u\Phi_\theta & 2\Phi_\theta \end{pmatrix}, \tag{17}$$

where $\Phi_\theta = \partial\Phi/\partial\theta$ etc. The Euler momentum flux $\Pi^{(0)} = 2E$ in the $\gamma = 3$ (or $D = 1$) case. The linear wave speeds, the eigenvalues of this matrix, are the three roots $\Lambda_- \le \Lambda_0 \le \Lambda_+$ of the cubic equation

$$\Lambda^3 + 2(u-\Lambda)\frac{\partial\Phi}{\partial u} - 2\left[\theta - (\Lambda-u)^2\right]\frac{\partial\Phi}{\partial\theta} - 2\Phi = 0. \tag{18}$$

The cubic does not factorise readily when Φ is given by eq. (15), compared with $\Lambda_0 = u$ and $\Lambda_\pm = u \pm \sqrt{\gamma\theta}$ for the Euler equations with $\Phi = u(p+E)/\rho = \frac{1}{2}u(u^2+3\theta)$. In particular, the system is not Galilean invariant as the wave speeds do not take the form $u-c$, u, $u+c$ for any sound speed c. This is because Φ involves terms like $\exp\left[-(\frac{3}{2} \pm u)/\theta\right]$.

The middle wave speed is linearly degenerate in the Euler equations, meaning that $\mathbf{r}_0 \cdot \nabla\Lambda_0 = 0$, where $\mathbf{r}_0$ is the right eigenvector of the Jacobian matrix (17) with eigenvalue Λ_0, and the gradient is taken with respect to the conserved variables $(\rho, \rho u, E)$ [12, 13]. The

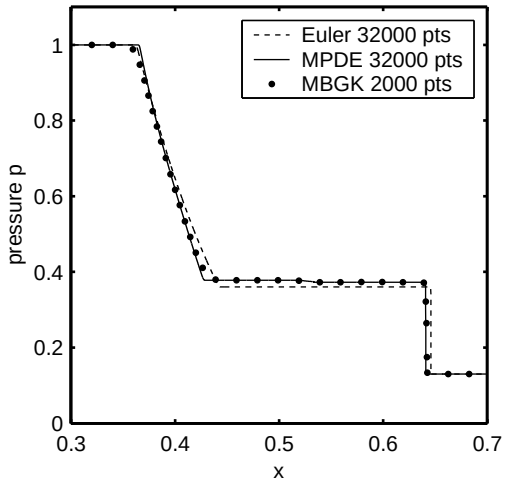

Fig. 1

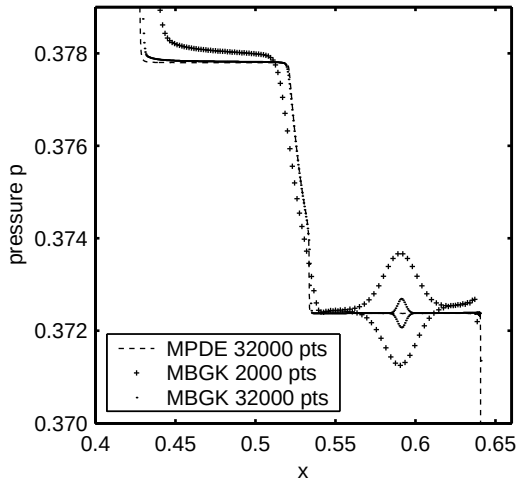

Fig. 2

Fig. 1 – Pressure at $t = 0.1$ with initial conditions from eq. (19). A slight discrepancy is visible between the Euler, and the MPDE and MBGK solutions. The pressure is a little too high between the shock and rarefaction, and the shock speed is a little too small.

Fig. 2 – Enlargement of Fig. 1 showing the MBGK scheme converging towards a solution of the MPDE equations instead of the Euler equations. The pressure is not uniform between the rarefaction and the shock in the MPDE and MBGK solutions. A small amplitude zig-zag mode is visible around $x = 0.6$, which decays as the grid is refined. The apparently double-valued MBGK solutions are due to the pressure at adjacent grid points being alternately above and below the true value.

corresponding wave is a contact discontinuity, meaning that the velocity and pressure are continuous, but a density jump may propagate with the linear wave speed $\Lambda_0 = u$. By contrast, the left and right waves are both genuinely nonlinear, meaning $\mathbf{r}_\pm \cdot \nabla \Lambda_\pm \neq 0$ always. The qualitative behaviour in a shock tube problem is therefore as illustrated in Fig. 1.1 of [12], or Fig. 6.5 of [14], with one shock, one rarefaction, and a contact discontinuity in the middle.

The middle wave in the MPDE system (16) is neither linearly degenerate nor genuinely nonlinear, since $\mathbf{r}_0 \cdot \nabla \Lambda_0$ may or may not vanish. Numerical solutions of the shock tube problems from [8] contain an unphysical compound wave, a shock attached to a rarefaction wave, instead of the contact discontinuity. The attachment point is marked by $\mathbf{r}_0 \cdot \nabla \Lambda_0 = 0$.

Numerical experiments. – As in [8], the lattice BGK simulations presented here used $\tau = 1$ in lattice units. Reference solutions were obtained by solving the Euler and MPDE hyperbolic systems on very fine grids, with up to 32000 points in the interval $0 \leq x \leq 1$, using the local Lax-Friedrichs scheme [12,13], and its second order accurate extension by Kurganov and Tadmor [19] for the figures. The latter is a semi-discrete scheme, and the ODE system was integrated with a second order, total variation diminishing, Runge-Kutta integrator [20]. These schemes do not require a solution of the Riemann problem, only the fluxes and a bound on the local wave speed, taken to be $|u| + \sqrt{\gamma\theta}$ as for the Euler equations. Boundary conditions were zero-gradient for these schemes, and periodic for the lattice BGK scheme. For the results shown no boundary influences had reached the waves emerging from $x = 0.5$.

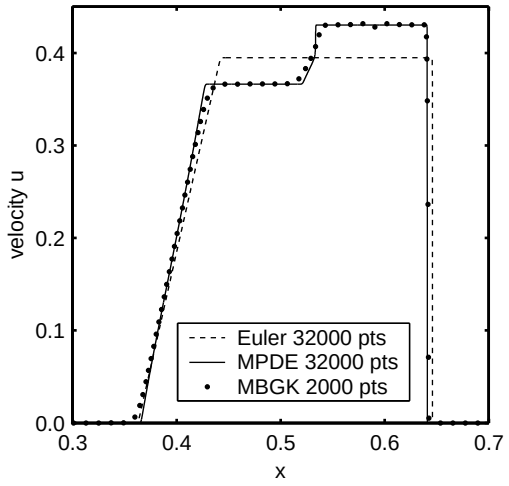

Fig. 3

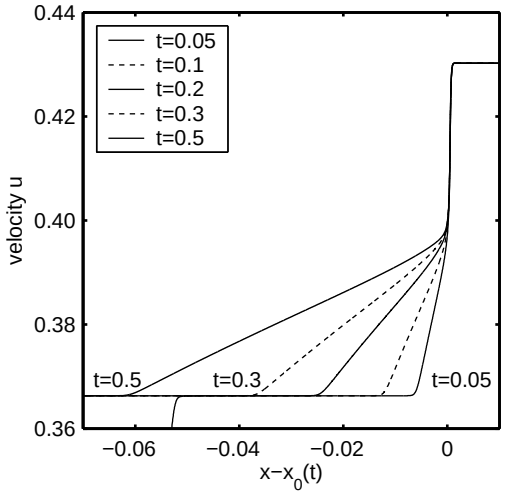

Fig. 4

Fig. 3 – Velocity at $t = 0.1$ with initial conditions from eq. (19). The MBGK and MPDE velocity is not uniform between the rarefaction and the shock, but the Euler velocity is uniform.

Fig. 4 – Velocity at various times showing the compound wave evolving. The profiles have been offset by varying displacements $x_0(t)$ to make the shocks coincide. The shock thickness stays uniform, as set by the numerical scheme, while the attached rarefaction wave expands linearly in time.

For the shock tube Riemann problem illustrated in Fig. 2 of [8], with initial data

$$\begin{array}{llll} \rho_{\rm L} = 1.6, & u_{\rm L} = 0.0, & p_{\rm L} = 1.0, & \text{for } x < 0.5, \\ \rho_{\rm R} = 0.4, & u_{\rm R} = 0.0, & p_{\rm R} = 0.12, & \text{for } x > 0.5, \end{array} \tag{19}$$

a discrepancy in the pressure is just about visible at $t = 0.1$ in our Fig. 1, versus $t = 0.02$ in Fig. 2 of [8]. Solutions of the Riemann problem should be self-similar in time, being functions of $(x - 0.5)/t$ only, but numerically there is an initial transient due to the initial data being represented on a discrete grid. Our Fig. 2 shows an enlargement of the region between the rarefaction wave and the shock, where the Euler solution has uniform pressure but the MPDE and MBGK solutions show pressure variations due to a compound wave (see below). A computational zig-zag instability is also visible around $x = 0.6$, the apparently multivalued solutions being due to pressures at adjacent grid points being alternately above and below the true solution.

The discrepancy between the Euler solutions and the MPDE and MBGK solutions is more prominent in the velocity, shown without enlargement in Fig. 3. The Euler velocity comprises three straight lines: the rarefaction, the horizontal line including the contact discontinuity, and the shock. The MPDE and MBGK solutions contain a third, compound wave in the middle. Figure 4 shows the velocity around $x = 0.5$ at various times from $t = 0.05$ to $t = 0.5$. The profiles are offset by varying amounts $x_0(t)$ so that the shocks coincide, while the attached rarefaction waves may be seen expanding out to the left. When plotted against $(x - 0.5)/t$ these profiles converge to a constant shape with a truely discontinuous shock.

The qualitative behaviour is identical for the other shock tube problem considered in [8], with $\rho_{\rm R} = 0.7$ and $p_{\rm R} = 0.25$. A compound wave is still prominent in the velocity, even for this weaker pressure jump, with an amplitude about 7% of the peak velocity. The pressure appears

almost uniform without enlargement, varying by only 0.2% across the compound wave. The MPDE energy flux $\rho\Phi$ from eq. (15) differs by a maximum of 3% from the correct Euler flux $\frac{1}{2}\rho u(u^3 + 3\theta)$, and by 7% for the stronger pressure jump in eq. (19). These discrepancies are much larger at higher temperatures, as is the discrepancy in shock speed just about visible in Fig. 1. In particular, the MPDE internal energy flux asymptotes to $\frac{17}{10}\rho u$ as $\theta \to \infty$, whereas the Euler internal energy flux $\frac{3}{2}\rho u\theta$ is proportional to θ.

Conclusion. – A lattice BGK scheme that is intended to simulate a thermal fluid at finite Mach numbers should reproduce the correct energy equation. At least the inviscid energy flux should be correct, and ideally the Fourier diffusive heat flux as well. This requires further constraints on moments of the equilibria over and above those required for a correct momentum equation, and over and above those proposed for "perfect entropies" in [10]. As the first few moments of the equilibria must be polynomials in $\mathbf{u}$, these constraints may be hard to satisfy with non-polynomial equilibria. The equilibria using an exact Maxwellian closure in [8] do not satisfy these constraints, and so simulate a different PDE system that admits compound waves where the Euler equations contain contact discontinuities. This may be rectifiable by choosing a different function in place of eq. (12), or by adding more speeds, but the polynomial equilibria of [21, 22] that attribute additional kinetic energies $\frac{1}{2}|\boldsymbol{\xi}_i|^2 + \epsilon_i$ to particles appear more promising, and have successfully simulated quite strong shocks.

* * *

The author thanks Hilary and John Ockendon for useful conversations. Financial support from St John's College, Cambridge, UK is gratefully acknowledged.

REFERENCES

[1] McNamara, G. and Zanetti, G., *Phys. Rev. Lett.*, **61** (1988) 2332
[2] Higuera, F. J., Succi, S. and Benzi, R., *Europhys. Lett.*, **9** (1989) 345
[3] Higuera, F. J. and Jimenez, J., *Europhys. Lett.*, **9** (1989) 663
[4] Qian, Y. H., d'Humières, D. and Lallemand, P., *Europhys. Lett.*, **17** (1992) 479
[5] Chen, S. and Doolen, G. D., *Annu. Rev. Fluid Mech.*, **30** (1998) 329
[6] De Cicco, M., Succi, S. and Bella, G., *SIAM J. Sci. Comput.*, **21** (1999) 366
[7] Boghosian, B. M., Yepez, J., Coveney, P. V. and Wagner, A., *Proc. R. Soc. Lond. A*, **457** (2001) 717
[8] Renda, A., Bella, G., Succi, S. and Karlin, I. V., *Europhys. Lett.*, **41** (1998) 279
[9] Karlin, I. V., Gorban, A. N., Succi, S. and Boffi, V., *Phys. Rev. Lett.*, **81** (1998) 6
[10] Karlin, I. V., Ferrante, A. and Öttinger, H. C., *Europhys. Lett.*, **47** (1999) 182
[11] Brio, M. and Wu, C. C., *J. Comput. Phys.*, **75** (1988) 400
[12] LeVeque, R. J., *Numerical Methods for Conservation Laws* 2nd ed. (Birkhäuser, Basel) 1992
[13] Godlewski, E. and Raviart, P.-A., *Numerical Approximation of Hyperbolic Systems of Conservation Laws* (Springer, New York) 1996
[14] Whitham, G. B., *Linear and Nonlinear Waves* (Wiley Interscience, New York) 1974
[15] Cercignani, C., *The Boltzmann Equations and its Applications* (Springer, New York) 1988
[16] Bhatnagar, P. L., Gross, E. P. and Krook, M., *Phys. Rev.*, **94** (1954) 511
[17] Dellar, P. J., *Phys. Rev. E*, **64** (2001) 031203
[18] Chen, Y., Ohashi, H. and Akiyama, M., *Phys. Rev. E*, **50** (1994) 2776
[19] Kurganov, A. and Tadmor, E., *J. Comput. Phys.*, **160** (2000) 241
[20] Shu, C.-W. and Osher, S., *J. Comput. Phys.*, **83** (1989) 32
[21] Yan, G. W., Chen, Y. S. and Hu, S. X., *Phys. Rev. E*, **59** (1999) 454
[22] Shi, W., Shyy, W. and Mei, R., *Num. Heat Transfer B*, **40** (2001) 1